KNACK: A Hybrid Spin-Charge Mixed-Mode Simulator for Evaluating Different Genres of Spin-Transfer Torque MRAM Bit-cells

Xuanyao Fong, Sumeet K. Gupta, Niladri N. Mojumder, Sri Harsha Choday, Charles Augustine, and Kaushik Roy
Department of Electrical and Computer Engineering, Purdue University, West Lafayette, IN 47907, USA
Email: {xfong, guptask, niladri, schoday, caugust, kaushik}@purdue.edu

***Abstract*—The storage device in spin-transfer torque MRAM (STT-MRAM) is the magnetic tunneling junction (MTJ) and several models for the MTJ have been proposed. However, a simulation framework that captures device physics at the atomistic level when simulating STT-MRAM at the bit-cell level is lacking. We propose a simulation framework (KNACK) which models the MTJ at the atomistic level using the Non-Equilibrium Green's Function (NEGF) formalism and uses the NEGF model in conjunction with our STT-MRAM bit-cell circuit model for circuit-level simulations. Our simulation framework accepts *I-V* and *C-V* characteristics of the access device input either as lookup tables or as compact models. We show that with appropriate device and bit-cell parameters, our simulation framework has the ability to capture MTJ physics and simulate different genres of STT-MRAM bit-cells with results in agreement with experiments.**

Spin-transfer torque; STT-MRAM; modeling; simulation framework; magnetic tunneling junction

I. INTRODUCTION

The emergence of spin-transfer torque magnetic random access memories (STT-MRAM) as a potential candidate for future universal memory technology resulted in significant research interest [1-5]. As a result, several genres of STT-MRAM bit-cells have been proposed in literature [2-5]. However, the evaluation of different genres of STT-MRAM bit-cells in different applications requires a simulation framework that has the ablility to capture the physics in the bit-cells during simulation. Such a simulation framework would allow comprehensive device-circuit-architecture analysis and co-optimization to achieve ultra-low power, high performance and robust STT-MRAM bit-cells.

A standard 1T-1R STT-MRAM bit-cell is shown in Fig. 1. The basic device in STT-MRAM bit-cells is the magnetic tunneling junction (MTJ). As shown in Fig. 1, the MTJ stack consists of two ferromagnetic layers sandwiching a tunneling oxide (either AlO_x or MgO). The ferromagnetic phenomenon in the ferromagnetic layers is due to exchange mediated alignment of electron spins in one direction. Experiments have demonstrated that the MTJ exhibits a tunneling resistance that depends on the relative magnetizations of its ferromagnetic layers [6-7]. Thus, the relative magnetization of the layers is used as the state variable in STT-MRAM bit-cells and can be sensed as the tunneling resistance of the MTJ.

Several models for the MTJ have been proposed in literature. Most of these models capture electronic transport in the MTJ and the magnetization dynamics of the MTJ separately. A common feature of these models is the fitting of MTJ characteristics using fitting functions instead of solving the transport equations for the MTJ structure. In our proposed simulation framework, we used an MTJ model that solves the transport equations using the Non-Equilibrium Green's Function (NEGF) formalism. This enables our simulation framework to capture device-physics at the atomistic-level when simulating STT-MRAM bit-cells at the circuit-level.

The following describes details of our simulation framework which we call KNACK. Section II describes the simulation flow of KNACK as well as the device and circuit-level models. KNACK was then used to simulate experimentally reported STT-MRAM bit-cells to demonstrate its capability. The simulation results are presented in Section III. Finally, Section IV concludes this paper.

II. SIMULATION FRAMEWORK DESCRIPTION

The overall simulation flow of KNACK is illustrated by the flowchart in Fig. 2. The simulation framework consists of 1) NEGF based electron transport model for MTJ, 2) Landau-Lifshitz-Gilbert (LLG) equation solver for capturing the free layer dynamics in MTJ, 3) a lookup table based model or compact model for the access device, and 4) circuit-level model to capture the behavior of the STT-MRAM bit-cell.

A. Circuit Model of STT-MRAM Bit-cell

The circuit model we propose for the STT-MRAM bit-cell is shown in Fig. 3. The bit- and source-line drivers are modeled as ideal voltage sources with output resistances R_{BS} and R_{SS}, respectively. With this circuit model, the strength of the bit- and source-line drivers can be controlled by varying R_{BS} and R_{SS}. Small output resistances (~1Ω) are used for strong drivers and large output resistances (~10MΩ) are used to put the driver in the high impedance state (or high-Z). This is useful for analyzing the use of voltage and current sensing schemes for reading STT-MRAM bit-cells. The word-line driver is modeled as an ideal voltage source. Stray capacitances on the bit- and source-lines, and the internal node, are included as C_{BL}, C_{SL} and C_{INT}, respectively. As reported in [2-3], the MTJ electrical behavior is like a variable resistor and we modeled it as such. With this circuit model for the bit-cell, the circuit behavior of the bit-cell is described by (1-3). When R_{BS}=0, KNACK ignores (1) and sets V_{BL}=V_{BD}. Similarly, (3) is ignored when R_{SS}=0 and V_{SL}=V_{SD}.

This research was funded in part by Nano Research Initiative (NRI), National Science Foundation (NSF), Intel Corp. and Qualcomm.

978-1-61284-418-3/11/$26.00 © 2011 IEEE

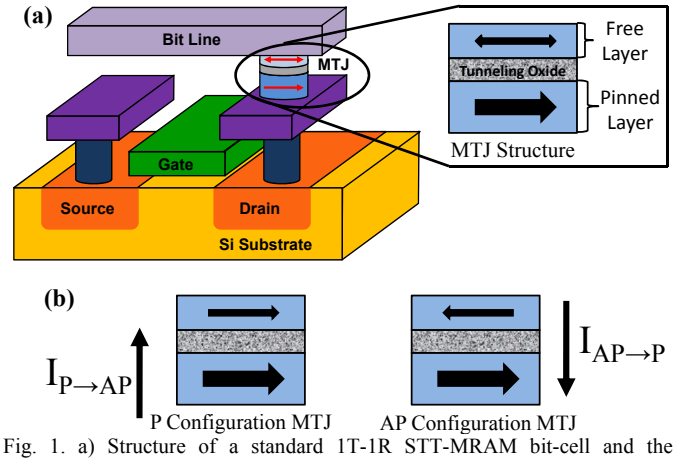

Fig. 1. a) Structure of a standard 1T-1R STT-MRAM bit-cell and the magnetic tunnel junction. b) MTJ configurations and the current directions and corresponding direction of magnetization reversal.

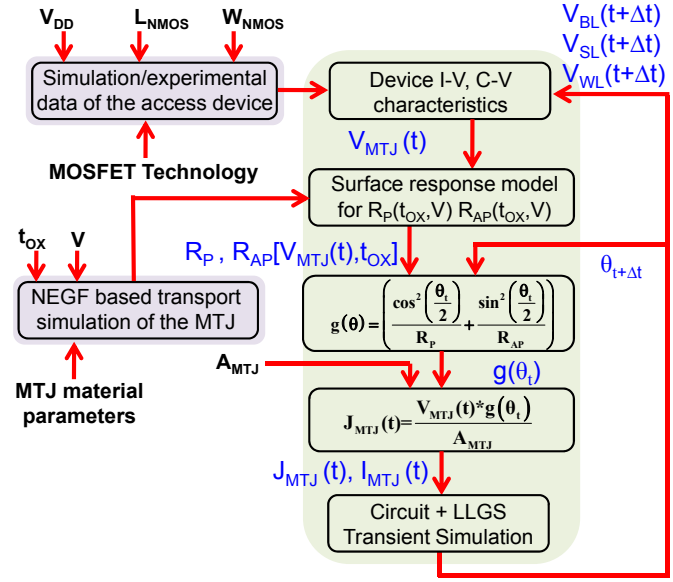

Fig. 2. Flow chart of our proposed simulation framework

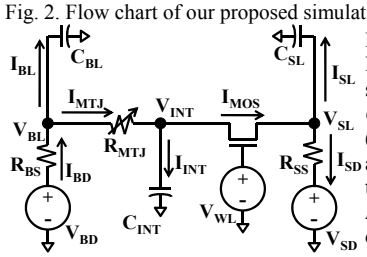

Fig. 3. Circuit model of STT-MRAM bit-cell with bit- and source-line capacitances (C_{BL} and C_{SL}), and internal node capacitance (C_{INT}). Bit- and source-line drivers are modeled as real voltage sources that can be made ideal (R_{BS}=0, R_{SS}=0) or tri-stated (R_{BS}=∞, R_{SS}=∞) during simulation.

In order to solve (1-3), the MTJ conductance $\left(G_{MTJ}=R_{MTJ}^{-1}\right)$ needs to be modeled. Since G_{MTJ} depends on the FL polarization [7], the FL dynamics needs to be solved. In nano-scale MTJ, the FL may be modeled as a mono-domain magnet. The magnetization dynamics in a mono-domain magnet is described by the Landau-Lifshitz-Gilbert (LLG) equation. The electronic transport in the MTJ is solved using the NEGF method.

B. The Landau-Lifshitz-Gilbert (LLG) Equation

During switching, G_{MTJ} varies as the current flowing through the MTJ and the relative angle between PL and FL change with time. Thus, the magnetization of the FL in the MTJ must be modeled in order to properly describe the MTJ dynamics. In scaled STT-MRAM bit-cell, the FL is a nano-magnet that can be modeled as a mono-domain magnet. Magnetization dynamics of a mono-domain can be obtained by solving the Landau-Lifshitz-Gilbert (LLG) equation, shown as (4) [8]. γ is the gyromagnetic ratio, α is the Gilbert damping ratio, $\hat{m}$ is the magnetization vector of the nano-magnet and $\overrightarrow{STT}$ is the spin-transfer torque term, and will be discussed in Section II-C.

Equation (5) shows how magnetic-field like interactions are included in our model. $\vec{H}_{uniaxial}$ is the uniaxial anisotropy field, $\vec{H}_{easy\text{-}plane}$ is the easy-plane anisotropy field, $\vec{H}_{applied}$ is the external magnetic field applied on the magnet, $\vec{H}_{dipolar}$ is the dipolar field from other magnets, and $\vec{H}_{fluct}$ is the thermal fluctuation field. The basis vectors for our coordinate system are $\hat{e}_x$, $\hat{e}_y$ and $\hat{e}_z$. We define the equilibrium direction of the magnet (or the easy axis) to be along the z-axis. This means that the magnetization vector ($\hat{m}$) is either $+\hat{e}_z$ or $-\hat{e}_z$ in equilibrium. The activation energy of the magnet, which determines the thermal stability of the magnet (E_A), is used to calculate the uniaxial anisotropy field using (6-7), where M_S and V are the saturation magnetization and volume of the magnet, respectively, and $E_A=Ku_2V$. Experiments have demonstrated $E_A \approx 67 k_BT$ for >10 years retention time, where k_B is the Boltzmann constant and T is the magnet temperature [1]. Equation (6) describes the demagnetizing field term for thin-film magnets with easy-plane anisotropy and applies to nano-magnets in which the easy axis is in the plane of the magnet. In our model, FL is in the x-z plane and electrons flow along the y-axis. However, recent experiments demonstrated nano-magnets with perpendicular magnetic anisotropy (PMA) [9]. PMA nano-magnets have their easy axis perpendicular to the plane of the magnet. In our model, a PMA FL is in the x-y plane and electrons flow along the z-axis. Anisotropy fields of a PMA magnet are modeled as (7). In an STT-MRAM array, the magnetizations of all the MTJs interact via dipolar interactions and may be captured using (8), where for the i-th nano-magnet, $\vec{r}_j$ is the vector from the nano-magnet to FL, $\hat{m}_j$ is the magnetization vector describing its orientation, and μ_r is the relative permeability of the material the nano-magnets and FL are buried in. Finally, the effect of finite temperature has been modeled as prescribed by Brown in [10] using (9-10), where the components of $\vec{H}_{fluct}$ are independent Gaussian random variables.

The spin-transfer torque term ($\overrightarrow{STT}$) depends on the current density flowing through the MTJ. We now show how KNACK uses the NEGF method to determine $\overrightarrow{STT}$.

C. Non-Equilibrium Green's Function Method

In order to describe FL magnetization dynamics under current-induced excitations, the spin-transfer torque term that enters LLG ($\overrightarrow{STT}$) needs to be calculated. Datta, Behin-Aein, Salahuddin and Datta [11] proposed using the Non-Equilibrium Green's Function (NEGF) formalism to rigorously treat effective mass based electronic transport and to calculate $\overrightarrow{STT}$. We first write the MTJ Hamiltonian ($\mathcal{H}$) as (17), where hI is the spin-independent part and $(\vec{\sigma}\cdot\hat{m})\Delta$ is the spin-dependent part arising from the exchange interaction with the nano-magnet point along $\hat{m}$. I is the identity matrix, $\vec{\sigma}$ represents the

Pauli spin matrices and Δ is the energy band splitting between up-spins and down-spins. Next, the divergence of spin current ($\vec{J}_S$) is calculated using (18). G^n is the correlation matrix and σ_k is the Pauli spin matrix along the k-direction (k = x, y, z) and $\hbar$ is the reduced Planck's constant. Finally, $\overrightarrow{STT}$ is calculated using (19).

The size of $\mathcal{H}$ may become prohibitively large when modeling large MTJs, increasing memory requirements of the simulation and simulation time. The use of mode space calculations to reduce the size of $\mathcal{H}$ while obtaining reasonably accurate results was proposed in [11]. The approach is to first write $\mathcal{H}$ in 1-D and compute the eigen-energies (λ_n) of the system. Equation (17) is modified and rewritten as (20). Equations (18-19) are evaluated using (20) to determine the contribution from each eigen-energy of interest. The contribution from each eigen-energy is finally summed up to obtain the result.

Alternatively, the spin-transfer torque term written by Xiao, Zangwill and Stiles in [12] is shown as (11). $\hat{p}$ is the unit vector in the direction of PL, q is the electronic charge, J_{MTJ} is the MTJ current density flowing from PL to FL, A_{MTJ} is the cross-sectional area and t_{FL} is the thickness of FL. $\hat{p}$ is set as $\hat{e}_z$ in KNACK for standard STT-MRAM bit-cell simulations. When (11) is used, the electronic transport within the MTJ is rigorously treated using NEGF by (21-23). Σ_k is the self-energy matrix describing the coupling of contact k of the MTJ to the external circuit, f_k is the Fermi function of electrode k. Using (23), the angle dependence of MTJ conductance $G_{MTJ}(\theta)=[R_{MTJ}(\theta)]^{-1}$ can be calculated and stored in a look-up table. Alternatively, R_{AP} and R_P as a function of MTJ voltage (V), the thickness of tunneling oxide (t_{OX}), and the angle between FL and PL magnetizations ($\theta=\cos^{-1}(\hat{m}\cdot\hat{p})$) can be calculated with $R_P=R_{MTJ}(0)$ and $R_{AP}=R_{MTJ}(\pi)$. R_{AP} and R_P as functions of V and t_{OX} are individually fitted to (24-25), where a_m, b_m, c and d are fitting parameters.

Solving NEGF equations is computationally expensive and slow [13]. The use of (21-25) to obtain a compact model for MTJ resistance enables accurate NEGF solution to electronic transport in the MTJ while significantly reducing STT-MRAM bit-cell simulation runtimes. It is then convenient to use (11) as the spin-transfer torque model. KNACK allows the user to specify whether to intensively solve NEGF for spin-transfer torque and electronic transport in the MTJ, or for solving electronic transport only. The user may also use KNACK to either generate look-up tables from NEGF parameters for use with (25) or to accept the look-up table generated by other means. The use of look-up tables is highly recommended to avoid repeating computationally expensive NEGF simulations when numerically integrating (1-4).

III. Simulation Results

Atomistic-level simulation (NEGF) in KNACK was first calibrated to published experimental data in [6] (Fig. 4). Magnetization dynamics simulation in KNACK is then benchmarked with OOMMF as shown in Fig. 5. Parameters used for Fig. 5 are M_S=850emu/cm^3, α=0.03, γ=17.6MHz/Oe, T=300K, $E_A=40k_BT$, t_{FL}=2.1nm, $P_L=P_R$=0.4 and $\Lambda_L=\Lambda_R$=2. After KNACK has been calibrated (Fig. 6), 1T-1R STT-MRAM bit-cells in standard and reverse connections were simulated [2]. The NEGF results were stored in a look up table for use in subsequent bit-cell simulations using the same MTJ. Fig. 7 shows the results of a KNACK simulation of a STT-MRAM bit-cell similar to the one reported in [3]. The access transistor used in the simulation is a 150nm wide NMOS transistor based on 45nm bulk CMOS technology. The LLG parameters for the FL are listed in Table II. The KNACK simulation results show worst-case bit-cell switching time of ~4.5ns for the standard-connected bit-cell and ~5.5ns for the reverse-connected bit-cell, in good agreement with experimental results obtained in [3].

IV. Conclusions

We proposed a hybrid spin-charge mixed-mode simulation framework (KNACK) for evaluating different genres of STT-MRAM bit-cells. We described the circuit-level STT-MRAM bit-cell model, and the device-level NEGF based and LLGS based models for MTJ electron transport and magnetization dynamics, respectively. KNACK was also shown to accept access device models in the form of either lookup tables or compact models. We also showed how KNACK simultaneously solves device and circuit-level model equations during circuit-level simulations so that device-circuit interactions are accurately captured. Finally, results from simulation of STT-MRAM bit-cells using KNACK are presented. It was shown that with appropriate simulation parameters, KNACK yielded results consistent with the experimentally reported results.

References

[1] Y. Huai, "Spin-transfer torque MRAM (STT-MRAM): challenges and prospects," *AAPS Bulletin* Vol 18 No 6, pp. 33-40, Dec 2008.

[2] C. J. Lin et al, "45nm low power CMOS logic compatible embedded STT MRAM utilizing a reverse-connection 1T/1MTJ cell," *IEDM '09*, pp. 279-282, Dec 2009.

[3] T. Kishi *et al*, "Lower-current and fast switching of a perpendicular TMR for high speed and high density spin-transfer-torque MRAM," *IEDM '08*, pp. 1-4, Dec 2008.

[4] N. N. Mojumder, S. K. Gupta, S. H. Choday, D. E. Nikonov, K. Roy, "A three-terminal dual-pillar STT-MRAM for high performance robust memory applications", *IEEE Trans. Electron Devices*, Vol. 58, No. 5, pp. 1508-1516, May 2011.

[5] N. N. Mojumder, K. Roy, "Switching current reduction and thermally induced delay spread reduction in tilted anisotropy spin-transfer torque MRAM," *IEEE Trans. Magn*., to be published.

[6] S. Yuasa, T. Nagahama, A. Fukujima, Y. Suzuki, K. Ando, "Giant room-temperature magnetoresistance in single-crystal Fe/MgO/Fe magnetic tunnel junctions," *Nature matl*, Vol. 3, pp. 868-871, Dec 2004.

[7] J. C. Sankey *et al*, "Measurement of the spin-transfer-torque vector in magnetic tunnel junctions," *Nature Phys.* Vol. 4, pp. 67-71, Jan 2008.

[8] T. L. Gilbert, "A phenomenological theory of damping in ferromagnetic materials," *IEEE Trans. Magn.* Vol 40, 6, pp. 3443-3449, Nov 2004.

[9] S. Ikeda *et al*, "A perpendicular-anisotropy CoFeB-MgO magnetic tunnel junction," *Nature Mat.* Vol. 9, pp. 721-724, Sep 2010.

[10] W. Brown Jr., "Thermal fluctuation of fine ferromagnetic particles," *IEEE Trans. Magn.* Vol 15, No. 5, pp. 1196-1208, Sep 1979.

[11] D. Datta, B. Behin-Aein, S. Salahuddin, S. Datta, "Quantitative Model for TMR and Spin-Transfer Torque in MTJ Devices," *IEDM 2010*, pp. 22.8.1-22.8.4, Dec 2010.

[12] J. Xiao, A. Zangwill, M. D. Stiles, "Boltzmann test of Slonczewski's theory of spin transfer torque," *Phys. Rev. B* Vol. 70, 172405, 2004.

[13] N. N. Mojumder, C. Augustine, D. E. Nikonov, K. Roy, "Electronic transport and effect of quantum confinement in dual barrier resonant tunneling spin-torque-transfer magnetic tunnel junctions," *Jour. Appl. Phys.* **108**, 104306, 2010.

TABLE I
SIMULATION FRAMEWORK EQUATIONS

Circuit: $\frac{dV_{BL}}{dt}=\frac{1}{C_{BL}}\left(G_{MTJ}V_{INT}+\frac{V_{BD}}{R_{BS}}-\left(\frac{1}{R_{BS}}+G_{MTJ}\right)V_{BL}\right)$ **(1)** $\frac{dV_{INT}}{dt}=\frac{1}{C_{INT}}\left(G_{MTJ}(V_{BL}-V_{INT})-I_{MOS}\right)$ **(2)** $\frac{dV_{SL}}{dt}=\frac{1}{C_{SL}}\left(\frac{V_{SD}-V_{INT}}{R_{BS}}+I_{MOS}\right)$ **(3)**

LLG: $\frac{d\hat{m}}{dt}=-|\gamma|\hat{m}\times\vec{H}_{EFF}-\alpha\hat{m}\times\hat{m}\times\vec{H}_{EFF}+\overrightarrow{STT}$ **(4)** $\vec{H}_{EFF}=\vec{H}_{uniaxial}+\vec{H}_{easy\text{-}plane}+\vec{H}_{applied}+\vec{H}_{dipolar}+\vec{H}_{fluct}$ **(5)**

In-plane anisotropy: $\vec{H}_{uniaxial}+\vec{H}_{easy\text{-}plane}=\frac{2Ku_2}{M_S}\hat{m}_z-4\pi M_S\hat{m}_y$ **(6)** Perpendicular anisotropy: $\vec{H}_{uniaxial}+\vec{H}_{easy\text{-}plane}=\left(\frac{2Ku_2}{M_S}-4\pi M_S\right)\hat{m}_z$ **(7)**

$\vec{H}_{dipolar,j}=\sum_i \mu_r\frac{3\left(\frac{M_{S,i}}{M_{S,j}}\hat{m}_i\vec{r}_i\right)-|\vec{r}_i|^2}{|\vec{r}_i|^6}\vec{r}_i$ **(8)** $\langle\vec{H}_{fluct,i}\rangle=0,\ i=x,y,z$ **(9)** $\langle\vec{H}_{fluct,i}(t)\vec{H}_{fluct,j}(t+\tau)\rangle=\frac{2\alpha k_BT}{|\gamma|M_SVol}\delta(\tau)\delta_{ij}$ **(10)** $\overrightarrow{STT}=\frac{\gamma g(\hat{m}\cdot\hat{p})J_{MTJ}}{2q\mu_0M_St_{FL}}(\hat{m}\times\hat{m}\times\hat{p}-\alpha\hat{m}\times\hat{p})$ **(11)**

$g(\hat{m}\cdot\hat{p})=\left[\frac{q_+}{A_+ +A_-\cos\theta}+\frac{q_-}{A_+ -A_-\cos\theta}\right]$ **(12)** $q_\pm=\left[P_{PL}\Lambda_{PL}^2\sqrt{\frac{\Lambda_{FL}^2+1}{\Lambda_{PL}^2+1}}\pm P_{FL}\Lambda_{FL}^2\sqrt{\frac{\Lambda_{PL}^2-1}{\Lambda_{FL}^2-1}}\right]$ **(13)** $A_\pm=\sqrt{(\Lambda_{PL}^2\pm1)(\Lambda_{FL}^2\pm1)}$ **(14)** $\Lambda^2=GR$ **(15)** $G=\frac{A_{MTJ}q^2k_F^2}{4\pi^2\hbar}$ **(16)**

NEGF: $\mathcal{H}=hI+(\vec{\sigma}\cdot\hat{m})\Delta$ **(17)** $[\vec{\nabla}\cdot\vec{J}_S]=\frac{1}{i\hbar}\int dE\{\mathrm{Trace}[\sigma_k(\mathcal{H}G^n-G^n\mathcal{H})]\}$ **(18)** $\overrightarrow{STT}=\frac{-\mu_B}{M_SV}\int dV\vec{\nabla}\cdot\vec{J}_S$ **(19)** $\mathcal{H}=hI+(\vec{\sigma}\cdot\hat{m})\Delta+\lambda_nI$ **(20)** $G=[EI-\mathcal{H}-\Sigma_{PL}-\Sigma_{FL}]^{-1}$ **(21)**

$\Gamma_k=i(\Sigma_k-\Sigma_k^\dagger)$, Σ_k=self-energy **(22)** $J_{MTJ}=\frac{q\int dE\{\mathrm{Trace}[\Gamma_{PL}G\Gamma_{FL}G^\dagger]\}(f_1-f_2)}{A_{MTJ}\hbar}$ **(23)**

$R\propto\left(e^{a_0t_{ox}+b_0}+\sum_{m=1}^{c}((-1)^{m-1}V^{2m}e^{a_mt_{ox}+b_m})\right)^{-d}$ **(24)**

$R(\theta)=\left(\frac{1}{R_P}\left(\cos\left(\frac{\theta}{2}\right)\right)^2+\frac{1}{R_{AP}}\left(\sin\left(\frac{\theta}{2}\right)\right)^2\right)^{-1}$ **(25)**

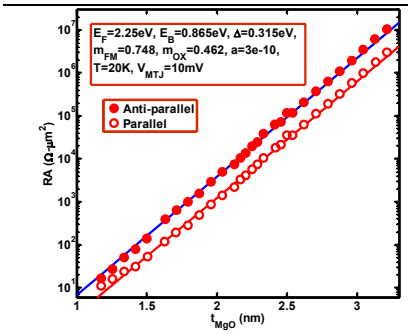

Fig. 4. NEGF simulation of MTJ resistance-area product was successfully calibrated in KNACK using the parameters listed (inset)

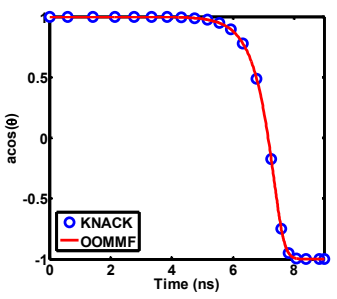

Fig. 5. Benchmarking of KNACK LLGS simulation against OOMMF

TABLE II
LLGS PARAMETERS FOR FIGURE 7

Activation Energy, E_A	$56k_BT$, T=300K
γ, α	17.6MHz/Oe, 0.028
Saturation magnetization, M_S	700emu/cm^3
Dimensions	$(\pi\times(25\mathrm{nm})^2)\times1.4$nm
$\overrightarrow{STT}$ Fitting Parameter, P, Λ	P_{PL}=0.8,P_{FL}=0.3, Λ_{PL}=Λ_{FL}=2

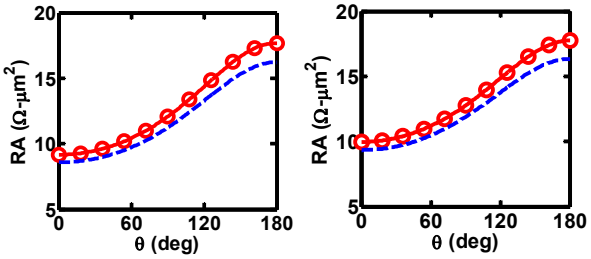

Fig. 6. The lines are plots of (14) for t_{MgO}=1.2nm. The MTJ voltage is 0.25V (top) and 0.3V (bottom). The circles were plotted using NEGF results and the line through them used RA_P and RA_{AP} from NEGF results. The dashed line was plotted using conductance look up table from fitting NEGF results to (13) first to obtain RA_P and RA_{AP}.

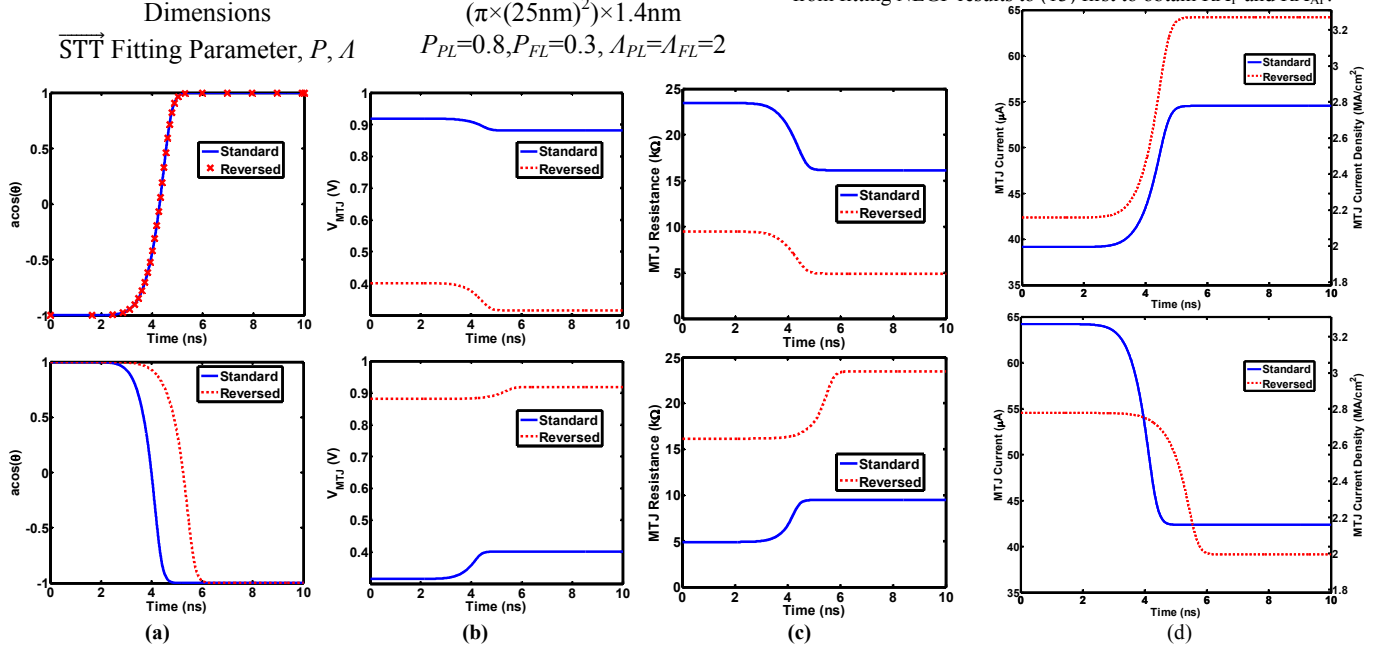

Fig. 7. Time evolution of 1T-1R STT-MRAM bit-cell parameters as simulated by KNACK. The top row illustrates switching from AP to P and the bottom row illustrates switching from P to AP. Time evolution of (a) the relative polarization angle (θ) of the free layer with respect to the pinned layer, (b) MTJ resistance, (c) MTJ voltage and (d) MTJ currents and current densities in standard- (solid) and reversed connected (dashed) STT-MRAM bit-cells. AP to P switching occurs faster than P to AP switching in both bit-cells. The bit-, source- and word-line voltages are held constant throughout these simulations.